A. Ghezzi, A. Farina, A. Bassi, G. Valentini, I. Labanca, G. Acconcia, I. Rech, and C. D'Andrea, "Multispectral compressive fluorescence lifetime imaging microscopy with a SPAD array detector," Opt. Lett. 46, 1353-1356 (2021).
https://doi.org/10.1364/OL.419381

Multispectral compressive fluorescence lifetime imaging microscopy with a SPAD array detector

Alberto Ghezzi[1,2,*], Andrea Farina[2], Andrea Bassi[1,2], Gianluca Valentini[1,2], Ivan Labanca[3], Giulia Acconcia[3], Ivan Rech[3], and Cosimo D'Andrea[1,4]

[1]Politecnico di Milano, Dipartimento di Fisica, Piazza L. da Vinci 32, 20133 Milan, Italy
[2]Consiglio Nazionale delle Ricerche, Istituto di Fotonica e Nanotecnologie, Piazza L. da Vinci 32, 20133 Milan, Italy;
[3]Politecnico di Milano, Dipartimento di Elettronica, Informazione e Bioingegneria, via Golgi 40, 20133 Milan, Italy
[4]Istituto Italiano di Tecnologia, Center for Nano Science and Technology, via Pascoli 70/3, 20133 Milano (Italy).
[*]Corresponding author: alberto.ghezzi@polimi.it

Abstract

Multispectral/hyperspectral Fluorescence Lifetime Imaging Microscopy (λFLIM) is a promising tool for studying functional and structural biological processes. The rich information content provided by a multidimensional dataset is often in contrast with the acquisition speed. In this work, we develop and experimentally demonstrate a wide-field λFLIM setup, based on a novel time-resolved 18x1 Single Photon Avalanche Diodes (SPAD) array detector working in a single pixel camera scheme, which parallelizes the spectral detection reducing the measurement time. The proposed system, which implements a single-pixel camera with compressive sensing scheme, represents an optimal microscopy framework towards the design of λFLIM setups.

Fluorescence lifetime imaging microscopy (FLIM) is a powerful, non-invasive, imaging tool which provides functional and structural information to study photophysical processes in biological samples [1] and nanomaterials [2]. In particular, FLIM is widely used to study biological processes in combination with genetically encoded fluorescent tags, and endogenous (e.g. NADH) fluorophores. Fluorescence lifetime is independent on excitation intensity and extremely sensitive to the fluorophore's microenvironment. Hence, it is well suited to probe local temperature, pH, metabolic state, ion concentration, and fluorescence resonance energy transfer (FRET) efficiency [3, 4]. Likewise, the fluorescence spectrum provides a fundamental fingerprint to discriminate different fluorophores [5]. For these reasons, spectrally resolved FLIM (λFLIM) technique, which combines spatial, spectral and temporal information, leads to an unprecedented sensitivity [6, 7] to draw a comprehensive picture of photophysical processes.

Biological specimens are intrinsically dynamical systems (e.g. metabolic processes), while many materials are subjected to photobleaching and, generally, a trade-off between acquisition time and information content has to be found. FLIM techniques are commonly based on two different schemes: (i) wide-field and (ii) raster scan. The first scheme allows for very fast measurements, but it generally shows limited spectral and temporal resolutions, while the second one allows for high spatial resolution at the cost of a long acquisition time, which is proportional to the number of pixels. Despite several optimizations and technological improvements devised throughout the years to reduce the measurement time (i.e. high speed scanners and highly sensitive detectors), the acquisition speed still remains a challenging issue.

In the last decade, the compressive sensing (CS) paradigm [8] has been introduced: a novel approach aiming at fully recovering information from an undersampled set of measurements. In classical signal processing, the number of elements to be acquired has at least to double the highest frequency component present in the signal spectrum. It has been mathematically proven that, when a signal has a sparse representation under a basis (e.g. Fourier, Wavelet, Hadamard, etc.), this limit can be overcome by recovering a signal with N degree of freedom using a set of $M \ll N$ measurements [9].

The main success of CS applied to imaging relies on the single-pixel camera (SPC) implementation [10].

When a 2D map of functional data must be acquired and 2D array detectors (e.g. CCD or CMOS cameras) are not appropriate, the SPC collects photons through a single-pixel detector measuring the inner product of the spatial distribution of light and a family of 2D test functions belonging to a complete basis set. The image is, afterwards, retrieved by solving a linear inverse problem with proper sparsity constrains. The nature and performances of the single-pixel detection system is a key aspect [11] for a multidimensional acquisition. In fact, it should provide spectral resolution, time resolution, ultimate sensitivity, or a combination thereof, which are not available in native 2D detectors. By applying CS to λFLIM it is possible to strongly reduce the acquisition time with minimum loss of information and a reduced amount of data to be transferred and processed. More recent approaches, capable of high-compression thanks to deep-learning strategies has been proposed for macroscopic field of view [12].

Multispectral fluorescence microscopy by means of a SPC, was firstly proposed by Studer et al. [13]. Recently, a macroscopic (field of view of a few centimeters) multispectral fluorescence lifetime imaging system has been proposed by Pian et al. [7] to address problems like diffuse optical tomography, molecular imaging and guided surgery [14]. The system by Pian et al. is based on a time-resolved spectrophotometer, which allows the parallel acquisition in spectrum and time. The detection device is based on a multichannel photomultiplier tube (PMT) (one channel for each spectral band) and a routing system, which is capable of encoding the channel detecting the photon. The routing system has inherently some drawbacks: firstly, the photon-counting statistics imposes a limitation on the overall count-rate over the channels ($\sim$1% of the pulsed laser source repetition-rate), secondly, two photons impinging simultaneously on the detector are discarded [15].

Improving parallelization among spectral channels leads to a higher photon harvesting efficiency and, consequently, to a further reduction of measurement time for a given signal-to-noise ratio (SNR). Recently, a high-performance single-photon avalanche diode (SPAD) 32$\times$1 linear array module designed with custom technology has been proposed by Peronio et al. [16]. This module features an array of SPAD detectors with 50 μm diameter, 250 μm of pitch, maximum count rate of 4×10^6 cps per channel and less than 20×10^3 cps of dark count rate at 25°C. The module embeds four eight-channel TCSPC boards, equipped with high performance 14-bit ADCs, working in parallel. The performances of the custom SPAD array are better than more common 2D CMOS SPAD matrices for quantum efficiency, temporal resolution and differential non-linearity of the converters [17]. In particular, quantum efficiency is higher in the green spectral region and it could be optimized for the red band, while CMOS are more sensitive in the blue region. Temporal resolution is about 30 ps, while for CMOS matrices is hundreds of picoseconds. Despite PMTs still represent a milestone in photon counting, in recent years SPADs have overtaken PMTs for better quantum efficiency, low working voltage, immunity to electromagnetic fields, compactness, scalability (in terms of chip dimension and integration in dense arrays) and robustness.

In this work we propose and experimentally validate a multispectral fluorescence lifetime imaging microscopy system based on the single-pixel camera approach combined with a novel SPAD linear array module.

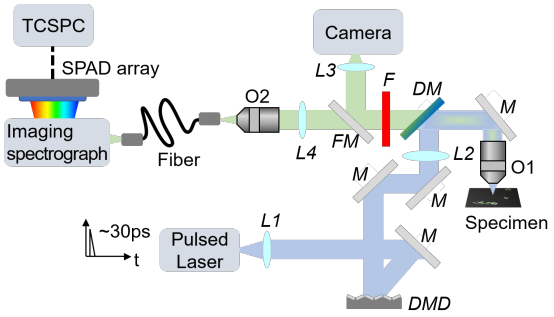

Figure 1: Experimental setup of the multispectral time-resolved wide-field single pixel fluorescence microscope. Legend: L = lens, M = mirror, DM = dichroic mirror, F = filter, FM = flip mirror, O = objective.

The setup is shown in Fig.1. It features a 40MHz mode-locked supercontinuum fiber laser (Fianium Inc., SC-450) emitting light pulses of about 30 ps, full width at half maximum (FWHM). The laser beam is spectrally filtered by a band-pass filter (10 nm FWHM) centered at 480 nm (FB480-10, Thorlabs, Inc.), coupled to a graded-index fiber (100 μm diameter) then expanded and projected by a lens (L1, f = 25 mm) on a Dig-

ital Micromirror Device (DMD, V-7000 ViaLUX GmbH). The DMD is a spatial light modulator constituted by an array (1024×768) of independently tiltable micromirrors, of size 13.7×13.7 μm^2 each. The modulated light is collected by a second lens (L2, f = 200 mm) and reflected by a dichroic mirror (DM, cut-on 505nm) towards an objective (O1, Plan N 40×/0.65 infinity corrected, Olympus Corp.). The microscope works in epi-fluorescence configuration. The collected fluorescence, selected by a long pass filter F (FEL500, Thorlabs, Inc.), can be addressed by a flip mirror (FM), either to a cooled 16-bit 512×512 charge-coupled device (CCD) camera (Versarray 512, Princeton Instruments) through a 200 mm tube lens (L3) or to the SPC. On the SPC side, the fluorescence signal is coupled into a step-index optical fiber (300 μm diameter, NA 0.4) through a lens (L4, f =150mm) and an objective (O2, Plan N 20×/0.40 infinity corrected, Olympus Corp.). The light from the distal end of the fiber is then focused on the entrance slit of an imaging spectrometer (Horiba CP140, f/2, 30nm/mm). The 32×1 SPAD array is placed in the output plane of the spectrometer for recording the spectrally- and time-resolved data. The field of view (FOV) is 140×140 μm^2. Out of the original 32 SPADs, 18 have been exploited for the current measurements.

The DMD modulates the light with a set of 1024 Scrambled Hadamard patterns, which are pseudo-random binary 32×32 matrices [18]. We obtained positive and negative entries by taking two measurements per pattern, with complementary binary pattern pairs, and taking the difference between them. Each element of the matrix involves 11×11 mirrors of the DMD which corresponds to a 4.4×4.4 μm^2 area on the sample. For a given illumination pattern, each measurement encodes part of the spatial information, and contains the average spectral-temporal information over the illuminated FOV.

Said $b_{\lambda,t}$ the vector of the $k = 1, \ldots, 1024$ measurements for the wavelength λ and the time bin t, and C a $k \times k$ sensing matrix of the used patterns, the unknown vector of the spatial distribution $a_{\lambda,t}$, which is resolved in time and wavelength, is retrieved by solving the linear problem $b = Ca$. This leads to a collection of as many bidimensional images, as the product of temporal and spectral elements. Combining the reconstructed images in a 4D matrix, each pixel of the stack contains the unmixed information in time and spectrum.

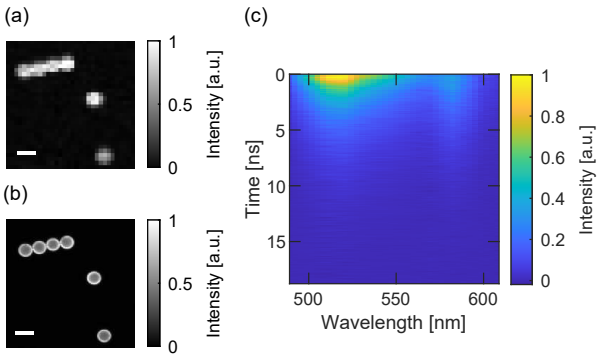

Figure 2: (a) Reconstruction of the FOV with 1024 patterns, from a spatial and temporal integration of the multidimensional SPC dataset. PSNR = 20.39 dB referred to the CCD image (b). Picture of the FOV taken with the CCD camera. The unit (white bar) is 20 μm. (c) Example of the spectral and temporal content from one pixel located in a bead.

We tested the multi-dimensional recording properties of our system on a microscope slide with microspheres of 15 μm diameter with fluorescent thin rings (FocalCheck F36909, Invitrogen). Each bead contains different fluorophores and, with 480 nm excitation wavelength, two of them (emitting at 515 nm and 580 nm, respectively) are simultaneously excited.

Each illumination pattern lasts for 200 ms, leading to a total measurement time of about 7 minutes, considering N = 1024 Scrambled Hadamard patterns. The illumination power on the sample is about 100 μW. At this value, when the DMD projects a flat, uniform pattern, the detector count-rate is 4×10^6 cps at the most highly illuminated SPAD detector, corresponding to a total count rate of 33.5×10^6 cps, considering the entire array.

Fig.2(a) shows the fluorescence intensity of the FOV, reconstructed from the multi-dimensional dataset by integrating over the entire spectral and temporal dimensions. We observe that the retrieved image is similar to the one captured by the CCD camera, which is show in Fig.2(b). The brightness of the bottom-

right bead is lower compared to the others due to slight inhomogeneity of the illumination profile. Yet, underneath each pixel of the intensity map in Fig.2(a), the entire spectral and temporal information is available, as shown in Fig.2(c). The counts for each spectral band, over 200 ms acquisition time, change from a minimum of 87×10^3 counts at 609 nm to a maximum of 83×10^4 counts at 520 nm.

In order to evaluate the quality of the reconstruction (i.e. the similarity between the reconstructed and CCD images) the peak signal-to-noise ratio (PSNR) is estimated. PSNR is defined [13] as $10log(d^2/MSE)$, where d is the dynamic range of the images, and MSE is the mean squared error between the reference and the reconstructed image. The PSNR is 20.39 dB for the image in Fig.2(a), which represents the baseline of the reconstruction quality for evaluating the robustness of the method when the number of measurements is reduced.

From the time/spectrum map in Fig.2(c), we observe the presence of two emission peaks around 515 nm and 580 nm, which correspond to different dyes. In order to retrieve the lifetime maps, the fluorescence decay in each pixel for each wavelength is fitted to a bi-exponential model, after applying a temporal binning of 20 ps to the raw data. The fits, over the pixels covering the region of the beads and in the spectral bands of the two dyes, give a bi-exponential decay with $\tau_1 = 0.84 \pm 0.17$ ns and $\tau_2 = 3.35 \pm 0.11$ ns ($A_1 = 31 \pm 5\%$ and $A_2 = 69 \pm 4\%$) for the dye emitting at the lower wavelength, and a mono-exponential decay with $\tau_3 = 3.86 \pm 0.15$ ns for the one emitting at the longer wavelength. In Fig.3 we show a synthetic representation of the fit results, where the retrieved lifetimes for two wavelengths in each pixel are reported as average lifetimes according to the following expression $\tau_M = A_1\tau_1 + A_2\tau_2$.

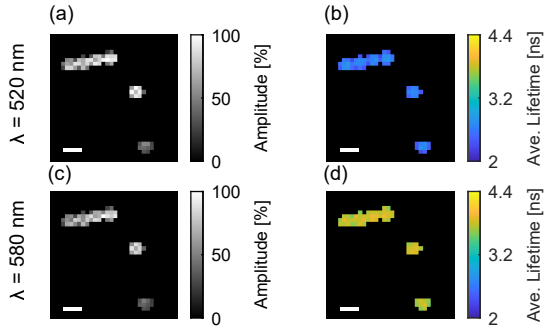

Figure 3: Fit results: (a) Amplitude of the decays normalized on the most intense pixel at 520 nm. (b) Average lifetimes at 520 nm.(c) Amplitudes normalized on the most intense pixel at 580 nm. (d) Average lifetimes at 580 nm. Scale bar: 20 μm.

Up to now, the image reconstruction has been carried out by using the whole scrambled Hadamard data set (M = N), which is a complete orthonormal basis set. To exploit the possibility of recovering the image by using a subset of M$\ll$N patterns (CS case), a random selection of M patterns out of the N available has been performed. Consequently, the linear problem becomes undetermined, ill-posed, and it has to be solved with regularization. The chosen reconstruction algorithm is the Total Variation Minimization by Augmented Lagrangian and Alternating Direction Algorithms (TVAL3)[19], a state-of-the-art solver in CS applications which is suitable for images with piecewise constant features [20, 21]. The reconstruction has been performed for each time and wavelength.

We considered different compression ratios (CR = 1-M/N) from 10% to 98% and calculated the PSNR at each step, assuming the CCD camera image as reference. TVAL3 parameters are optimized to obtain the highest possible PSNR per each compression ratio. The corresponding CR 0% is the one shown in Fig.2(a). The PSNR analysis is reported in Fig.4(a) and it can be seen that, remarkably, up to CR 70% the PSNR is constant around 20.6 $\pm$ 0.1 dB, demonstrating the spatial redundancy of the dataset. Afterwards, at CR 90% the image quality drops of about 0.4 dB with respect to average value of the cited range, however, the contrast of the beads over the background is still high and allows a clear discrimination among them. For higher compressions, the image quality rapidly worsens, and it becomes difficult to recognize the beads without some *a priori* information, like a camera image.

In Fig.4 (b)-(c) two examples of reconstructed images at CR 80% and 90%, respectively, are shown. It is worth noting that, up to CR 90%, the spectral and temporal shapes are not significantly affected by compression. Fig.4(d) shows the normalized emission spectrum (integrated over time) at three different CRs (70%, 80% and 90%) and non-compressed one (in blue) showing a similar behavior. The same agreement

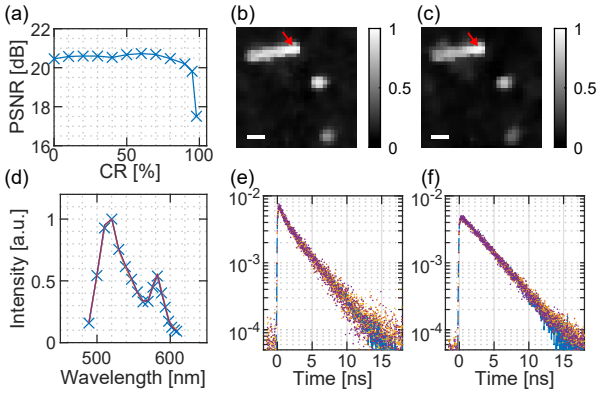

Figure 4: PSNR is reported at different compression ratio (a). The reconstructed SPC images at different compression ratios are shown at 80% (b) and 90% (c), respectively. Scale bar: 20 μm. The emission spectrum extracted from a pixel (identified by the red arrow in (b)) (d). The uncompressed dataset is in blue, CR 70% (red), CR 80% (yellow) and CR 90% (purple). The temporal decay extracted from the same pixel relatively to peak at 515 nm (over 30 nm) (e) and 580 nm (over 20 nm) (f).

is also observed for the temporal dimension, as shown in Fig.4(e) for the bi-exponential decays at lower wavelengths and Fig.4(f) for the mono-exponential decay at longer wavelengths. Therefore, by applying a CR 90% it is possible to strongly reduce the acquired dataset and, consequently, the measurement time which, in our case, is reduced to 42 seconds, with only a small loss of spatial details in the reconstruction, as reported by PSNR of 20.20 dB.

Thanks to the high parallelism of the detector array, which increases the counting efficiency, we can reach the reported count rate of 33.5×10^6 cps, that is much higher than a traditional single router-based multispectral counting system limit ($\sim$1x10^6 cps). The better counting efficiency leads to a reduction of the integration time, for a given illumination power and SNR.

With the proposed system, it is possible to strongly reduce the total measurement time. This perspective is promising for *in vivo* cellular studies and intravital microscopy, and in general for applications where fast acquisition is needed because of the dynamical changes of the biological sample or when light exposure should be limited due to photobleaching. Moreover, in many cases, it is possible to devise strategies for merging low-resolution multi-dimensional dataset with high-resolution CW data to obtain a high-resolution hypercube. This possibility will be investigated in a future work. The main limiting factor is represented by the low fill factor of the SPAD, which reduces the light harvesting efficiency. The low fill factor is given by the small dimension of each detector (a diameter of 50 μm) and the pitch between adjacent elements (250 μm). However, the custom SPAD technology allows us to build larger diodes, e.g. of 200 μm diameter [22] with a pitch of 250 μm. Thus, a 16 times improvement in light-harvesting efficiency is expected only by geometrical aspects. Consequently, this can be exploited to further reduce the acquisition time and/or illumination power and/or to rise the spatial resolution by increasing the number of patterns according to the characteristics of the specific sample and application. Furthermore, the use of a microlens array and additional cooling system can be used respectively to further increase the light harvesting and reduce the dark count rate.

In conclusion, in this work, to the best of our knowledge, we present and experimentally demonstrate the first scheme for compressive λFLIM microscopy based on single-pixel camera scheme, coupled to a custom time-resolved 18x1 SPAD array. We believe that the proposed scheme is highly promising towards the design and development of a fast multidimensional fluorescence lifetime microscopy. Furthermore, the use of wide field spatial modulated light can be well adapted to exploit different strategies simultaneously such as optical sectioning [23] and multi-photon microscopy [24] in combination with FLIM. Future work will be devoted to further reducing the acquisition time by developing SPAD arrays with larger detection area and novel compressive sensing algorithms to reach higher compressions, aiming at faster acquisition for biological and material science applications.

Funding

Regione Lombardia project NEWMED (co-financed with resources of POR FESR 2014-2020), ERC Starting Grant SOLENALGAE (679814), LASERLAB-EUROPE V (grant agreement no.871124, H2020) and Bi-lateral project CNR-Royal Society of London (3710).

Disclosures

The authors declare no conflicts of interest.

Supplementary Material

Details on the 32x1 SPAD array The developed detection module consists of two units [16]: a detection head and a TCSPC board. The two modules are connected by means of a Samtec cable made of 32 pairs of coupled coaxial cables allowing the transmission of the timing information between the two units. The detection module hosts the SPAD detectors in a sealed chamber, the front-end electronics and dedicated power supply networks to generate the numerous bias voltages needed for the detectors, the quenching and readout electronics and the temperature control system based on a Peltier cell. The SPAD chip is a 32x1 array of detectors built in custom technology in order to have good detection efficiency (50% at 550nm), low dark count rates (average count rate of 400c/s at 10 °C) and high time resolution (< 65ps FWHM including the electronics). The diameter of each SPAD is 50um while the pitch between the detectors is 250um. The front end consisting of a pseudo n-MOS inverter is integrated within the same chip in order to minimize the capacitive load, which is paramount to collect the avalanche current for timing purposes. The output of the front-end is fed to an array of integrated comparators built in 0.35 μm CMOS technology providing LVDS (low-voltage differential signaling) outputs. The detection head provides both a counting and a timing output for each detector. The Counting output is generated by the integrated Active Quenching Circuits (AQCs) and routed towards an internal FPGA that manages the data processing and communication via USB directly towards the PC. On the contrary, the Timing output generated from the integrated comparators is buffered and then sent to the TCSPC module. Here, the timing signals coming from the detection head are used as STARTs of the TCSPC module while the STOP is provided by the end user and it is common to all channels. The 32 timing signals are handled by 4 identical 8-channel board. Each board features 2 arrays of time-amplitude converters (TACs) with picosecond resolution developed in SiGe 0.35um technology, an 8-input ADC and a FPGA that stores the ADC data and manages the dithering technique. The four cards merge the data into a high-speed USB 2.0 hub. The system has a single DC power supply (8-16V) and a consumption of about 30W. Each channel can convert 4MHz signals thus generating up to 128 Mega conversions per second. The module is connected to a computer via a USB 3.0 interface. We exploit such array geometry to detect the line-shaped spectrum relayed by the spectrometer.

References

[1] Xiongbo Liu, Danying Lin, Wolfgang Becker, Jingjing Niu, Bin Yu, Liwei Liu, and Junle Qu. Fast fluorescence lifetime imaging techniques: A review on challenge and development. *Journal of Innovative Optical Health Sciences*, 12(5):1–27, 2019.

[2] Edward S Barnard, Eric T Hoke, Stephen T Connor, James R Groves, Tevye Kuykendall, Zewu Yan, Eric C Samulon, Edith D Bourret-Courchesne, Shaul Aloni, P James Schuck, Craig H Peters, and Brian E Hardin. Probing carrier lifetimes in photovoltaic materials using subsurface two-photon microscopy. *Scientific Reports*, 3(1):2098, 2013.

[3] Rupsa Datta, Tiffany M. Heaster, Joe T. Sharick, Amani A. Gillette, and Melissa C. Skala. Fluorescence lifetime imaging microscopy: fundamentals and advances in instrumentation, analysis, and applications. *Journal of Biomedical Optics*, 25(07):1, 2020.

[4] Francesco Mascia, Laura Girolomoni, Marcelo J. P. Alcocer, Ilaria Bargigia, Federico Perozeni, Stefano Cazzaniga, Giulio Cerullo, Cosimo D'Andrea, and Matteo Ballottari. Functional analysis of photosynthetic pigment binding complexes in the green alga haematococcus pluvialis reveals distribution of astaxanthin in photosystems. *Scientific Reports*, 7(1):16319, Nov 2017.

[5] Liang Gao and R. Theodore Smith. Optical hyperspectral imaging in microscopy and spectroscopy – A review of data acquisition. *Journal of Biophotonics*, 8(6):441–456, 2015.

[6] Florian Rousset, Nicolas Ducros, Françoise Peyrin, Gianluca Valentini, Cosimo D'Andrea, and Andrea Farina. Time-resolved multispectral imaging based on an adaptive single-pixel camera. *Optics Express*, 26(8):10550, apr 2018.

[7] Qi Pian, Ruoyang Yao, Nattawut Sinsuebphon, and Xavier Intes. Compressive hyperspectral time-resolved wide-field fluorescence lifetime imaging. *Nature Photonics*, 11(7):411–414, jul 2017.

[8] E.J. Candes and M.B. Wakin. An Introduction To Compressive Sampling. *IEEE Signal Processing Magazine*, 25(2):21–30, mar 2008.

[9] David L. Donoho. Compressed sensing. *IEEE Transactions on Information Theory*, 52(4):1289–1306, apr 2006.

[10] Marco F. Duarte, Mark A. Davenport, Dharmpal Takhar, Jason N. Laska, Ting Sun, Kevin F. Kelly, and Richard G. Baraniuk. Single-pixel imaging via compressive sampling. *IEEE Signal Processing Magazine*, 25(2):83–91, mar 2008.

[11] N. Radwell, K.J. Mitchell, G.M. Gibson, M.P. Edgar, R. Bowman, and M.J. Padgett. Single-pixel infrared and visible microscope. *Optica*, 1(5):285–289, 2014.

[12] M. Ochoa, A. Rudkouskaya, R. Yao, P. Yan, M. Barroso, and X. Intes. High compression deep learning based single-pixel hyperspectral macroscopic fluorescence lifetime imaging in vivo. *Biomed. Opt. Express*, 11(10):5401–5424, Oct 2020.

[13] Vincent Studer, Jérome Bobin, Makhlad Chahida, Hamed Shams Mousavia, Emmanuel Candes, and Maxime Dahane. Compressive fluorescence microscopy for biological and hyperspectral imaging. *Proceedings of the National Academy of Sciences of the United States of America*, 109(26):1679–1687, 2012.

[14] Andrea Farina, Marta Betcke, Laura di Sieno, Andrea Bassi, Nicolas Ducros, Antonio Pifferi, Gianluca Valentini, Simon Arridge, and Cosimo D'Andrea. Multiple-view diffuse optical tomography system based on time-domain compressive measurements. *Opt. Lett.*, 42(14):2822–2825, Jul 2017.

[15] Joseph R. Lakowicz. *Principles of Fluorescence Spectroscopy*. Springer US, Boston, MA, jan 2006.

[16] P. Peronio, I. Labanca, G. Acconcia, A. Ruggeri, A. A. Lavdas, A. A. Hicks, P. P. Pramstaller, M. Ghioni, and I. Rech. 32-Channel Time-Correlated-Single-Photon-Counting System for High-Throughput Lifetime Imaging. *Review of Scientific Instruments*, 88(8), 2017.

[17] S Antonioli, L Miari, A Cuccato, M Crotti, I Rech, and M Ghioni. 8-channel acquisition system for time-correlated single-photon counting. *Review of Scientific Instruments*, 84(6):64705, jun 2013.

[18] L Gan, T T Do, and T D Tran. Fast compressive imaging using scrambled block Hadamard ensemble. In *2008 16th European Signal Processing Conference*, pages 1–5, aug 2008.

[19] Chengbo Li, Wotao Yin, Hong Jiang, and Yin Zhang. An efficient augmented Lagrangian method with applications to total variation minimization. *Computational Optimization and Applications*, 56(3):507–530, 2013.

[20] M. Ochoa, Q. Pian, R. Yao, N. Ducros, and X. Intes. Assessing patterns for compressive fluorescence lifetime imaging. *Optics Letters*, 43(18):4370, 2018.

[21] N. Pavillon and N.I. Smith. Compressed sensing laser scanning microscopy. *Optics Express*, 24(26):30038–30052, 2016.

[22] Massimo Ghioni, Angelo Gulinatti, Ivan Rech, Piera Maccagnani, and Sergio Cova. Large-area low-jitter silicon single photon avalanche diodes. *Quantum Sensing and Nanophotonic Devices V*, 6900(February):69001D, 2008.

[23] Yuehao Wu, Peng Ye, Iftekhar O. Mirza, Gonzalo R. Arce, and Dennis W. Prather. Experimental demonstration of an Optical-Sectioning Compressive Sensing Microscope (CSM). *Optics Express*, 18(24):24565, 2010.

[24] Milad Alemohammad, Jaewook Shin, Dung N. Tran, Jasper R. Stroud, Sang Peter Chin, Trac D. Tran, and Mark A. Foster. Widefield compressive multiphoton microscopy. *Optics Letters*, 43(12):2989, 2018.